

## Article

# An Experimental and Numerical Study of Abrupt Changes in Coal Permeability with Gas Flowing through Fracture-Pore Structure

Lin Li <sup>1,2,3,4,5</sup>, Shufan Zhang <sup>1</sup>, Zhiqiang Li <sup>1,2,3,4</sup>, Xiangjun Chen <sup>1,2,3,4,\*</sup>, Lin Wang <sup>1,2,3,4</sup> and Shuailong Feng <sup>1</sup><sup>1</sup> College of Safety Science and Engineering, Henan Polytechnic University, Jiaozuo 454003, China<sup>2</sup> MOE Engineering Center of Mine Disaster Prevention and Rescue, Henan Polytechnic University, Jiaozuo 454003, China<sup>3</sup> Collaborative Innovation Center of Coal Work Safety and Clean High Efficiency Utilization, Henan Polytechnic University, Jiaozuo 454003, China<sup>4</sup> Henan Provincial Key Lab of Gas Geology and Control-Cultivation Base of Provincial and Ministry Joint State Key, Henan Polytechnic University, Jiaozuo 454003, China<sup>5</sup> State Key Laboratory Cultivation Base for Gas Geology and Gas Control (Henan Polytechnic University), Henan Polytechnic University, Jiaozuo 454003, China

\* Correspondence: chenxj@hpu.edu.cn

**Abstract:** Coal permeability is related to the fracture-pore structure of coal and is a key factor in determining gas drainage efficiency. The characteristics of the methane flow in coal fractures are different from those in coal matrix pores. However, due to the difficulty of observing fast methane flow in coal fractures, the effect of gas flow in coal fractures on coal permeability has seldom been considered and investigated. In this study, a cylindrical coal sample is used for the measurement of coal permeability under different gas pressures, and an abrupt change in coal permeability evolution was observed. Then, a tandem fracture-pore permeability model was adopted to analyze these new methane flow phenomena. In this permeability model, the deformation of coal fractures was directly analyzed and modeled without the reversed derivation. With the consideration of elastic modulus of coal fractures, the deformation of coal fractures is controlled by the effective strain of coal fractures, the adsorption-induced strain and effective strain of coal matrix. The research results show that (1) coal fractures quickly and significantly influence coal permeability by resisting coal deformation; (2) a complete evolution of coal permeability consists of the fast permeability change caused by methane flow in coal fractures and the slow permeability change caused by methane flow in coal matrix; (3) the low efficiency of gas mass exchange between coal fractures and coal matrix leads to a two-stage evolution for gas desorption flow and coal permeability.

**Keywords:** fractures; matrix; deformation; methane; permeability

**Citation:** Li, L.; Zhang, S.; Li, Z.; Chen, X.; Wang, L.; Feng, S. An Experimental and Numerical Study of Abrupt Changes in Coal Permeability with Gas Flowing through Fracture-Pore Structure. *Energies* **2022**, *15*, 7842. <https://doi.org/10.3390/en15217842>

Academic Editors: Zhenyuan Yin and Shuxia Li

Received: 28 August 2022

Accepted: 26 September 2022

Published: 22 October 2022

**Publisher's Note:** MDPI stays neutral with regard to jurisdictional claims in published maps and institutional affiliations.



**Copyright:** © 2022 by the authors. Licensee MDPI, Basel, Switzerland. This article is an open access article distributed under the terms and conditions of the Creative Commons Attribution (CC BY) license (<https://creativecommons.org/licenses/by/4.0/>).

## 1. Introduction

Coalbed methane (CBM) is a clean fuel and has attracted much attention for development. Permeability is a key factor in assessing CBM development and methane drainage. With the increase in coal mining depth, coal of higher rank is extracted with lower coal permeability, resulting in huge challenges to methane drainage improvement [1–3]. The change in coal permeability can be influenced by gas pressure, confining the pressure, adsorption capacity and mechanical properties of coal [4–8]. As a result, it is not easy to explain the complex evolution of coal permeability. Generally, CBM development is limited by low coal permeability. Due to the low coal permeability, more time and measures are needed for improvements in methane drainage, which is vital for coal mining safety and gas production [9,10]. However, long-time methane drainage will slow coal mining. To take effective measures to enhance coal permeability and shorten the methane drainage process, understanding the characteristics of gas flow in coal and the change in coal permeability is important for improving this situation. Meantime, the change of coal permeability is vital

when gas, such as carbon dioxide, is injected into reservoirs, such as coalbeds, to form gas hydrate for gas storage. The formation of gas hydrate usually needs a high gas pressure under appropriate temperature. When gas is injected into reservoirs, the increasing gas pressure changes reservoir permeability, which will influence the gas injection process. Therefore, it is necessary to understand the change of reservoir permeability for better gas drainage and injection. Gas movements in coal are complex due to the fracture-pore structure of coal. Typically, coal is considered to be a dual-pore medium with coal fractures and micro pores in coal matrix [11–13]. However, there are no uniform standards and critical values for distinguishing coal fractures and pores. The pore size in coal varies from nanometer to micrometer, and the micro pores in coal matrix significantly contribute to coal porosity [14–16]. Gas movement in small channels, like coal matrix pores, is slow and can be described by molecular diffusion, Knudsen diffusion and surface diffusion [17–20]. Darcy's law is usually adopted to describe methane flow in coal fractures [7,13,21]. According to Darcy's law, the fluid flow rate is determined by pressure gradient, coal permeability and fluid viscosity. As Darcy's law is proposed based on the water flow through beds of sand, the difference in fluid properties between liquid and gas should be considered. For example, the phenomenon of gas slippage at the pore wall is different from the boundary layer theory for liquid [18]. Much methane can adsorb on and desorb from pore walls in the coal matrix, and this causes coal deformation to influence gas flow. For example, during methane drainage, methane desorbs from pore walls in the coal matrix and flows to coal fractures. Due to gas desorption, the coal matrix will shrink to increase the volume of coal fractures, and this increases resistance for methane to flow out from the coal matrix. On the contrary, during gas injection, gas moves into the coal matrix pores through coal fractures. Due to gas sorption, the coal matrix swells to reduce the volume of coal fractures, and this increases resistance for methane to flow in from coal fractures [7,22]. Mojgan found that the injection of CO<sub>2</sub> can cause coal matrix swelling to reduce coal permeability when CO<sub>2</sub> pressure is above 1.5 MPa [23]. Based on the experimental results, coal matrix deformation is considered a main influence on coal permeability [24].

To figure out the evolution of coal permeability during the methane drainage and gas injection processes under stress-loading conditions, many coal permeability models are developed based on the experimental results [11,25]. Typically, the steady-state method is adopted for the measurement of coal permeability. With a simple experimental set-up and a straightforward analytical solution, this method is believed to reflect the methane flow in coal fracture systems [11,26,27]. To measure the low permeability of tight cores, unsteady state methods are usually adopted for this goal [11,28,29]. For porous coal, coal fractures are the main channels for methane flow, while the coal matrix is the main space for methane storage. Yun established a numerical simulation mathematical model with the consideration of oil–water–gas phase equilibrium to study the rapid flow of gas in fractured reservoirs [30]. Based on the dual-pore characteristic of coal, a match stick model was proposed to simulate the pore structure of coal [7,21,25]. In this model, the coal matrix was the match stick and the void space between them stood for coal fractures. Coal matrix and coal fractures can deform to change coal porosity and coal permeability when gas pressure changes. Under the constant confining stress condition, coal deformation is mainly determined by the adsorption-induced strain and effective strain. Based on the definition of porosity and stress–strain relationships, the stress–permeability relationship can be determined [22,31]. During a gas injection process, an increasing gas pressure broadens coal fractures to increase the aperture of coal fractures. Meanwhile, the coal matrix expands to decrease the aperture of coal fractures as gas absorbs on coal [7,22]. In a gas drainage process, a pressure drop decreases the aperture of coal fractures because of the compression effect of confining stress, and the coal matrix shrinks to increase the aperture of coal fractures due to gas desorption [1,22]. Harpalani found that coal permeability decreases with the reduction of gas pressure in coal pores [32]. In these two processes, the gas pressure in coal fractures changes fast while it changes slowly in coal matrix [7,22,33].

Furthermore, the coal matrix and coal fractures have opposite deformation to change coal porosity, which causes complex changes in coal permeability [7,22].

In previous research, the influence of gas flow in the coal matrix on the evolution of coal permeability was studied extensively. As gas flow changes quickly in coal fractures, it is not easy to experimentally observe [11,22]. As a result, the effect of gas flow in coal fractures on coal permeability is investigated insufficiently. To investigate a complete change process of coal permeability including the influence of coal fractures, in this study, a cylindrical coal sample is used to measure coal permeability under different gas adsorption equilibrium pressures. Then, by directly describing the deformation of coal fractures without any reversed derivation, a tandem fracture-pore permeability model is proposed for studying the methane flows in coal fractures and the coal matrix for analyzing the changes in coal permeability. Finally, this proposed model is used to investigate the evolution of coal permeability under gas drainage condition for explaining a challenge for CBM development.

## 2. Experimental Methodology

To study the effect of gas flows in coal fractures and the coal matrix on coal permeability, an experiment was conducted to record the desorption flow volume of methane from a cylindrical coal. A meta-anthracite sample was collected from the coal mining area of Guhanshan, Jiaozuo, China. The measured basic parameters of the Guhanshan coal samples are shown in Table 1. The coal sample was prepared as a cylinder with a height of 10 cm and a diameter of 5 cm. It was sealed by a rubber sealing stripe after 2 h of drying at the temperature of 353 K before the test. The experimental platform, shown in Figure 1, mainly consists of the gas injection unit, stress loading unit and measuring unit.

**Table 1.** Basic parameters of the Guhanshan coal.

Parameters	Values
Moisture	0.035
Ash	0.081
Volatile matter	0.055
Density/ $\text{g}\cdot\text{cm}^{-3}$	1.56
Porosity	0.041
a (Langmuir constant)/ $\text{cm}^3\cdot\text{g}^{-1}$	41.70
b (Langmuir constant)/ $\text{MPa}^{-1}$	1.50

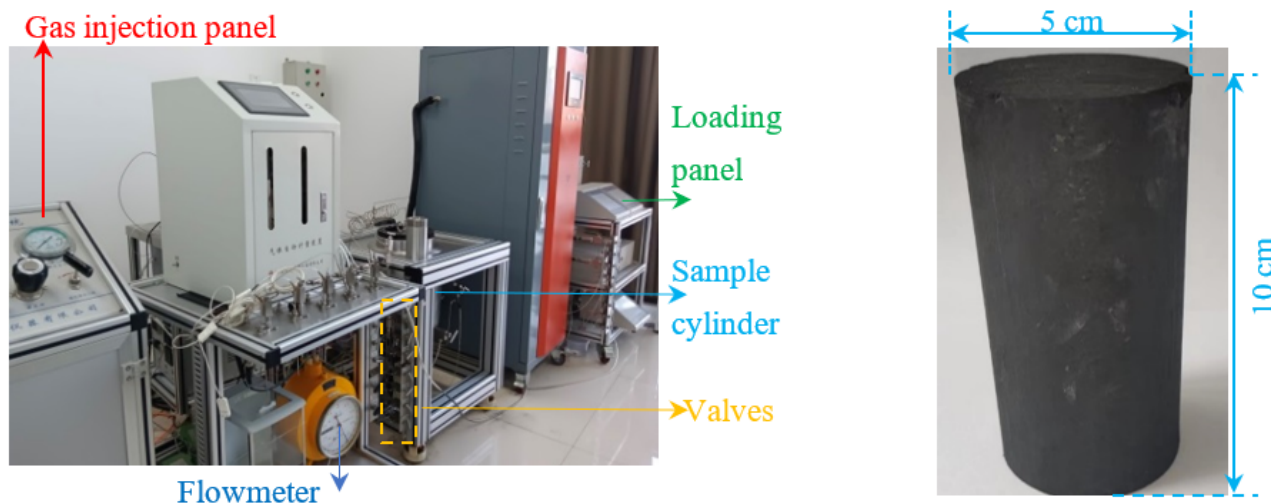


**Figure 1.** Experimental platform and coal sample.

Firstly, the coal sample was wrapped in a rubber envelope and placed in the sample cylinder. Secondly, with other valves closed and valves 3 and 4 open, this coal sample was degassed by starting the vacuum pump till the pressure gauge read 10 Pa. After that, valve 4 was closed. Thirdly, the confining pressure was set to 12 MPa, while the axial pressure was 6 MPa. The confining pressure was realized by adjusting the pressure of the oil filling the sample cylinder. The axial pressure was realized by adjusting the water pressure that presses on the metal at the head and tail of the coal sample. Then, different gas adsorption equilibrium pressures for the cylindrical coal sample were achieved. By opening and closing valves 1, 2 and 3 with other closed valves, the methane of the pre-set pressure was injected into this sealed coal sample, and the gas pressure decreased as gas adsorption proceeded. Repeat these operations until the adsorption equilibrium is reached under 0.5 MPa, 1 MPa and 1.5 MPa. This process took 96 hours to reach the adsorption equilibrium. Finally, the measurement of desorption flow volume of methane started. The desorption flow volume of methane was recorded by a flowmeter for 180 min once the system was connected to the atmosphere. The experimental platform structure can be found in Figure 2.

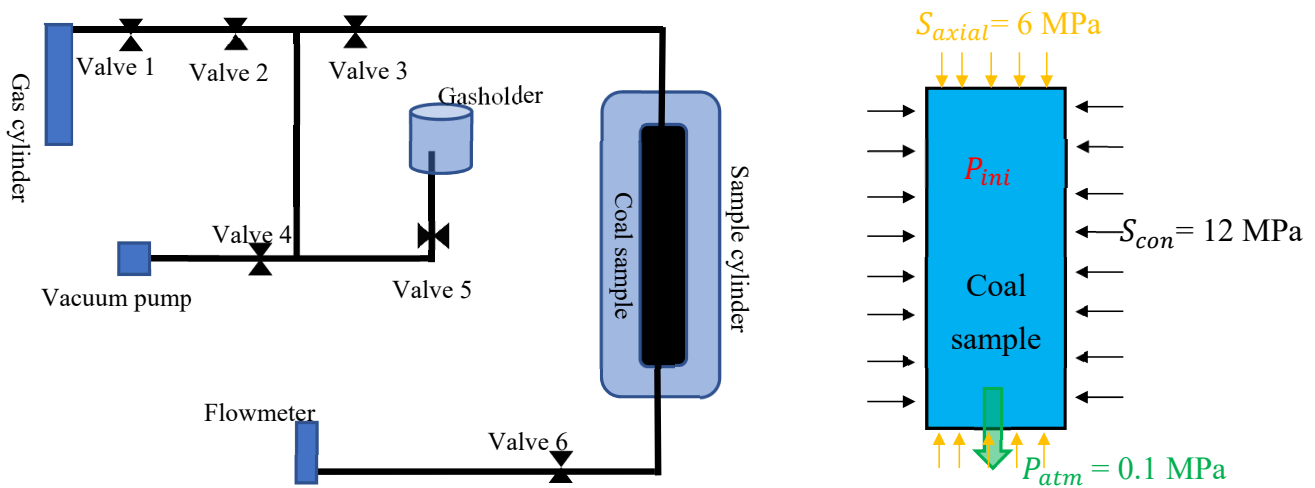


Figure 2. Experimental platform structure and Experimental set-up.

### 3. Conceptual Model

The match stick model developed from the dual-pore reservoir, shown in Figure 3, was adopted as the basis to construct a tandem fracture-pore permeability model for coal [7,34]. In this tandem fracture-pore permeability model, methane is assumed to migrate from small pores to big pores in the coal matrix and finally to coal fractures [19,34]. A porous solid medium can be considered to consist of ‘hard’ and ‘soft’ portions [35–37]. The solid, the fluid and the pore space in a porous medium have strength against deformation [38]. As a kind of porous medium in which pores are formed during the formation of coal under the metamorphism, coal has fracture structure and coal matrix to simultaneously resist deformation. The overall strength of coal is determined by the strength of the coal matrix and the structure of coal fractures [35,37]. As the series springs shown in Figure 4, coal fractures and the coal matrix are considered to be in series to resist deformation. With the bulk moduli of coal and the coal matrix, the bulk modulus of coal fractures can be determined by the below equation [37]:

$$\frac{1}{K} = \frac{\phi_f}{K_f} + \frac{1}{K_m} \quad (1)$$

where  $K$  is the bulk modulus of coal;  $K_f$  is the bulk modulus of coal fractures;  $K_m$  is the bulk modulus of the coal matrix and  $\phi_f$  is the porosity of coal fractures.

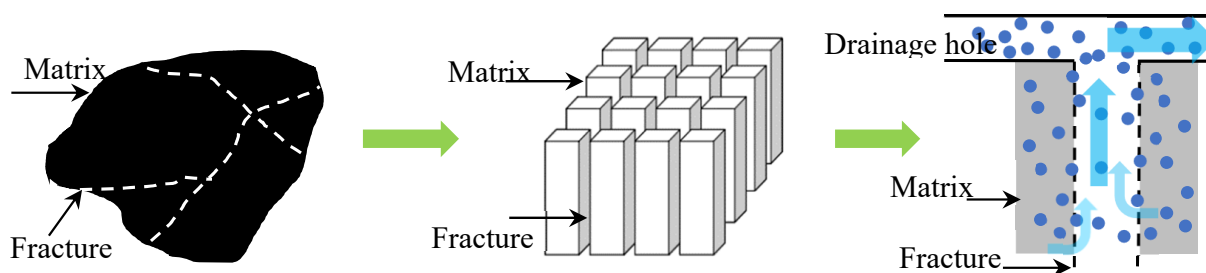


Figure 3. Illustration of the series methane flow in the dual-pore coal.

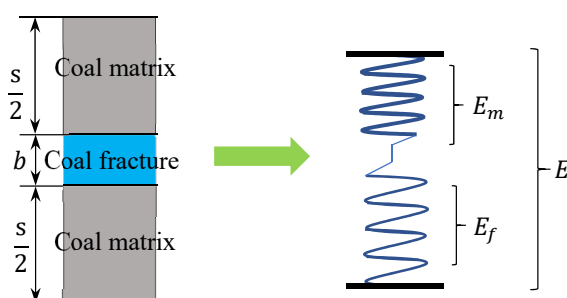


Figure 4. Series structure of coal fractures and coal matrix.

With the bulk moduli of coal, coal matrix and coal fractures, the effective strain of coal fractures and the coal matrix can be determined based on the principle of effective stress. Meantime, gas flows cause a change in gas pressures, which leads to coal deformation due to the adsorption-induced expansion and desorption-induced shrinkage [7,22]. If there is an increase in gas pressure in coal, coal fractures will be broadened and coal matrix will swell. On the contrary, coal fractures will be narrowed and the coal matrix will shrink when there is a decrease in gas pressure in coal. Changes in the gas pressures in coal impose two-sided impacts on coal deformation, which leads to the complex evolution of coal permeability. Due to the fast change in gas pressure in coal fractures and slow change of gas pressure in the coal matrix, the evolution of coal permeability can be inferred to experience fast changes at the initial stage and gradual changes at the later stage.

Due to the varying physical properties and adsorption capacity of different coal, the deformation of coal fractures and the coal matrix can be different even under the same conditions of confining stress and gas pressure. As a result, coal permeability shows different change routines in a coal permeability map. However, with a reasonable coal permeability model, the change in coal permeability for a selected coal can be investigated and predicted under different conditions.

#### 4. Numerical Modelling

The evolution of coal permeability is determined by the change in coal porosity with the cubic law between coal porosity and coal permeability, which is related to the physical properties of coal, effective strain and adsorption strain [7,22,31]. Under a stable confining stress, the gas pressure is an important factor for investigating the effective strain and adsorption strain, and changes in gas pressure can be determined by studying the methane flow in coal. In this research, two sets of equations that describe methane flow and coal deformation are built for coal fractures and the coal matrix to study the effect of gas flow on coal permeability.

##### 4.1. Methane Flow in Coal

Based on the ultra-slow outflow of methane in the coal matrix and the limited surface of drainage holes, the methane migration in coal is assumed to be a series flow in which methane moves from the coal matrix to coal fractures and finally to drainage holes. Methane

flows in coal fractures and the coal matrix satisfy both the mass conservation law and Darcy's law [18,39]. The bridge between these two flows is the mass exchange of methane. For a process of gas injection and gas drainage, gas flow in coal fractures first reaches the equilibrium state, and then gas migrates slowly in coal matrix. The pressure equilibrium in the coal matrix usually needs a long time due to the slow mass exchange between coal fractures and coal matrix [27,28,31].

For a methane flow in coal fractures, the mass conservation equation and the momentum conservation equation are described as below [7,21]:

$$\frac{\partial m_f}{\partial t} - \nabla \cdot (\rho_f \frac{k_f}{\mu} \nabla p_f) = Q_b \quad (2)$$

$$m_f = \rho_f \phi_f \quad (3)$$

where  $m_f$  is the mass of methane in coal fractures;  $\rho_f$  is the methane density in coal fractures;  $k_f$  is the coal fracture permeability;  $\mu$  is the methane viscosity;  $p_f$  is the pressure in coal fractures;  $\phi_f$  is the porosity of coal fractures; and  $Q_b$  is the exchange mass of methane between coal fractures and the coal matrix, which can be determined by the below equation [12,33]:

$$Q_b = \omega(p_m - p_f) = \gamma(p_m - p_f) \frac{k_m}{\mu} \rho_m \quad (4)$$

where  $\gamma$  is the matrix-fracture transfer shape factor,  $p_m$  is the pressure in coal matrix;  $k_m$  is the permeability of coal matrix; and  $\rho_m$  is the methane density in the coal matrix.

The methane flow in the coal matrix needs to satisfy the mass conservation equation and the momentum conservation equation that are described below [7]:

$$\frac{\partial m_m}{\partial t} - \nabla \cdot (\rho_m \frac{k_m}{\mu} \nabla p_m) = -Q_b \quad (5)$$

$$m_m = \rho_m \phi_m \quad (6)$$

where  $m_m$  is the mass of methane in the coal matrix and  $\phi_m$  is the porosity of the coal matrix.

In the above equations, coal permeability and coal porosity are two vital variables. For a selected coal, these two variables are influenced by coal deformation that is determined by the mechanical properties of coal, adsorption-induced strain and effective strain, which is analyzed in detail in the next section. Based on Darcy's law, methane flow in coal fractures that are directly connected to the drainage hole is faster with its big permeability and big pressure differential. On the contrary, methane flow in the coal matrix is slow because the pressure gradually changes in coal matrix due to its low permeability.

## 4.2. Deformation of Coal

### 4.2.1. Deformation of Coal Fractures

Gas flows cause changes in gas pressure, and this leads to coal deformation due to effective strain and adsorption-induced strain. Coal deformation includes changes in the volumes of coal fractures and coal matrix [7,22,31]. In this study, the deformation of coal fractures is analyzed based on the fluid environment and the loading environment that it is in. The change in the aperture of coal fractures is influenced by the effective strain of coal fractures, adsorption-induced strain of the coal matrix and effective strain of the coal matrix. Based on the effective stress theory, the increase in gas pressure in coal fractures reduces the compression of coal fractures, broadening the aperture of a coal fracture. However, the increasing gas pressure in coal matrix reduces the compression of coal matrix, which decreases the aperture of coal fractures [7,22,31]. Additionally, the increasing gas pressure increases the methane adsorption in the coal matrix to cause the swelling of the coal matrix, resulting in the shrinkage of coal fractures. The deformation equation of coal fractures is not derived from the deformation of coal matrix and bulk coal. This is different because many

other permeability models determining coal fracture deformation using the derivation of coal and the coal matrix may ignore the deformation characteristics of coal fractures. With the determined bulk modulus of coal fractures in Equation (1), the change in the aperture of coal fractures can be calculated by the below equation:

$$\Delta b = \Delta \varepsilon_{bet} b_0 - \frac{\Delta \varepsilon_s}{3} s_0 + \Delta \varepsilon_{set} s_0 \quad (7)$$

where  $b_0$  is the initial aperture of a coal fracture;  $s_0$  is the initial width of coal matrix;  $\varepsilon_{bet}$  is the effective strain of a coal fracture;  $\varepsilon_s$  is the adsorption-induced strain of coal matrix; and  $\varepsilon_{set}$  is the effective strain of coal matrix.

The effective strain of coal fractures is calculated by the below equation:

$$\varepsilon_{bet} = \frac{\sigma - p_f}{E_f} \quad (8)$$

where  $\sigma$  is the confining stress;  $p_f$  is the pressure in coal fractures; and  $E_f$  is Young's modulus of coal fractures, which can be obtained from Equation (1).

The adsorption-induced strain and effective strain of coal matrix can be calculated by the below equations [22]:

$$\varepsilon_s = \varepsilon_L \frac{p_m}{p_m + P_L} \quad (9)$$

$$\varepsilon_{set} = \frac{\sigma - p_m}{E_m} \quad (10)$$

where  $\varepsilon_L$  is the Langmuir volumetric strain constant;  $p_m$  is the Langmuir pressure constant; and  $E_m$  is Young's modulus of coal matrix.

Based on the definition of porosity, the porosity of coal fractures is calculated by the below equation:

$$\phi_f = \frac{3b}{s + 3b} \quad (11)$$

where  $b$  is the aperture of a coal fracture;  $s$  is the width of the coal matrix.

Based on Equation (7), the strain of coal fractures can be described as below [7]:

$$\varepsilon_f = \frac{\Delta b}{b_0} = \Delta \varepsilon_{bet} - \frac{s_0}{3b_0} (\Delta \varepsilon_s - 3\Delta \varepsilon_{set}) = \Delta \varepsilon_{bet} - \left( \frac{1}{\phi_{f0}} - 1 \right) (\Delta \varepsilon_s - 3\Delta \varepsilon_{set}) \quad (12)$$

With the strain of coal fractures, the change in the porosity of coal fractures can be described as below [22]:

$$\frac{\phi_f}{\phi_{f0}} = \left( 1 + \frac{\Delta b}{b_0} \right) \frac{s_0 + 3b_0}{s + 3b} = \frac{1 + \varepsilon_f}{1 + \varepsilon_m (1 - \phi_{f0}) + \phi_{f0} \varepsilon_f} \quad (13)$$

$$\varepsilon_m = \frac{\Delta \varepsilon_s}{3} - \Delta \varepsilon_{set} \quad (14)$$

Based on the changing porosity of coal fractures, the evolution of coal fracture permeability can be determined with the cubic law as below [22]:

$$\frac{k_f}{k_{f0}} = \left( \frac{\phi_f}{\phi_{f0}} \right)^3 \quad (15)$$

#### 4.2.2. Deformation of Coal Matrix

Coal matrix is considered to be a homogeneous, isotropic and elastic continuum for model simplification [7]. Based on the elastic theory for a porous medium, the stress-strain relationship for the coal matrix can be written as below [31]:

$$\varepsilon_{ij} = \frac{1}{2G_m} \sigma_{ij} - \left( \frac{1}{6G_m} - \frac{1}{9K_m} \right) \sigma_{kk} \delta_{ij} + \frac{\alpha}{3K_m} p_m \delta_{ij} + \frac{\varepsilon_s}{3} \delta_{ij} \quad (16)$$

where  $G_m$  and  $K_m$  are the shear modulus and bulk modulus of coal matrix;  $\alpha$  is the Biot coefficient;  $\sigma_{kk}$  is the total stress;  $\delta_{ij}$  is the Kronecker delta;  $p_m$  is the pressure in coal matrix; and  $\varepsilon_s$  is the adsorption-induced strain of coal matrix.

Considering the principle of effective stress and adsorption-induced strain, Equation (16) can be further simplified as below [7]:

$$\varepsilon_v = -\frac{1}{K_m} (\bar{\sigma} - \alpha p_m) + \varepsilon_s \quad (17)$$

where  $\varepsilon_v = \varepsilon_{11} + \varepsilon_{22} + \varepsilon_{33}$  is the volumetric strain of coal matrix and  $\bar{\sigma} = \frac{\sigma_{kk}}{3}$  is the mean compressive stress.

The coal matrix volume,  $V$ , is assumed to consist of the solid volume,  $V_s$ , and pore volume,  $V_p$ . The porosity of coal matrix can be described as below [7]:

$$\phi_m = \frac{V_p}{V_p + V_s} = \frac{V_p}{V} \quad (18)$$

Based on Equation (17), the below relationships can be obtained [38]:

$$\frac{\Delta V}{V} = -\frac{1}{K_m} (\Delta \bar{\sigma} - \alpha \Delta p) + \Delta \varepsilon_s \quad (19)$$

$$\frac{\Delta V_p}{V_p} = -\frac{1}{K_p} (\Delta \bar{\sigma} - \beta \Delta p) + \Delta \varepsilon_s \quad (20)$$

where  $\beta = 1 - \frac{K_p}{K_s}$ .

Solving Equations (18)–(20), the change in the porosity of coal matrix can be obtained as below [7]:

$$\Delta \phi_m = \phi_m - \phi_{m0} = \Delta \left( \frac{V_p}{V} \right) = \phi_{m0} \left( \frac{1}{K_m} - \frac{1}{K_p} \right) (\Delta \bar{\sigma} - \Delta p_m) = -(\alpha - \phi_{m0}) \frac{(\Delta \bar{\sigma} - \Delta p_m)}{K_m} \quad (21)$$

Ignoring the influence of  $\frac{(\Delta \bar{\sigma} - \Delta p_m)}{K_m}$ , Equation (21) can be simplified into

$$\frac{\phi_m}{\phi_{m0}} = 1 - \frac{\alpha}{\phi_{m0}} \frac{(\Delta \bar{\sigma} - \Delta p_m)}{K_m} \quad (22)$$

Based on the cubic law, the permeability of coal matrix is determined as below [22]:

$$\frac{k_m}{k_{m0}} = \left( \frac{\phi_m}{\phi_{m0}} \right)^3 \quad (23)$$

By building the above equations for methane flows and coal deformation, a tandem fracture-pore permeability model for coal was constructed in this study. The influence of gas pressures in coal fractures and the coal matrix is reflected in this permeability model. With Young's modulus of coal fractures, the influence of methane flow in coal fractures on coal permeability can be further analyzed.



## 5. Results and Discussion

### 5.1. Model Validation

In this study, the ratio of the accumulative desorption flow volume of methane to the total desorption volume is used to describe the experimental results. The experimental results for adsorption equilibrium pressures of 0.5 MPa, 1.0 MPa and 1.5 MPa are shown in Figure 5. It is clear that the desorption flow process can be divided into two stages like two line segments connecting with an inflection point. Under the adsorption equilibrium pressure of 1.5 MPa, at the first stage, the desorption flow volume of methane quickly increases to 1.2% of the total desorption flow volume with a sharp slope in the first 6 min. Then, the desorption flow volume of methane slowly increases by another 1.8% at the second stage of 174 min. Under the adsorption equilibrium pressures of 1.0 MPa and 0.5 MPa, the desorption flow ratios at the first stage are 1.25% and 1.7%, respectively. The desorption flow ratios at the first stage are 1.75% and 1.5%, respectively.

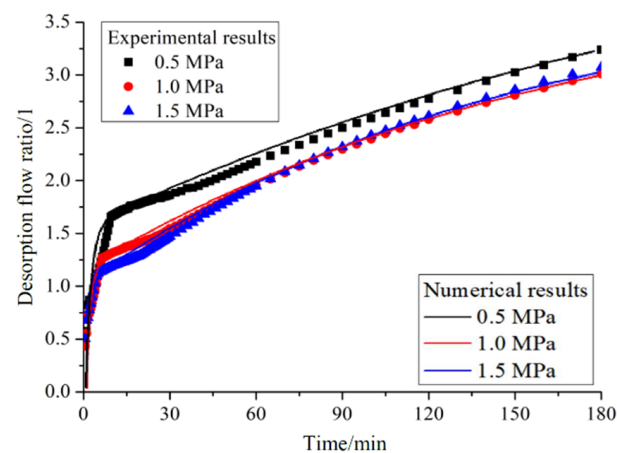


**Figure 5.** Experimental results of methane desorption flow for Guhanshan coal.

The numerical simulation results are shown with experimental results in Figure 5. To avoid repeating the analysis, the results under the adsorption equilibrium pressure of 1.5 MPa are selected as a representative as shown in Figure 6. The basic parameters for Guhanshan coal in the experimental and numerical research are listed in Table 2. With the numerical simulation results that are close to the experimental results, the tandem fracture-pore permeability model was used to analyze the changes caused by methane flows in Guhanshan coal. Coal holds methane in the form of gas compression in coal fractures and gas sorption in the coal matrix. The permeability of coal fractures can be several orders of magnitude greater than that in the coal matrix due to the differences in pore size. For Guhanshan coal, in the 6 min of the first stage, the limited methane stored in coal fractures flows out of coal sample in a high speed as the red line shown in Figure 6d. the gas flow velocity reaches the maximum of  $1.78 \times 10^{-5}$  m/s from zero in a very short time. Then, the gas flow in coal fractures quickly slow down to the minimum of  $0.025 \times 10^{-5}$  m/s. As a result, the gas pressure in coal fractures decrease quickly from 1.5 MPa to 0.1 MPa, as the green line shown in Figure 6c. Based on Terzaghi's principle, these changes cause a fast increase in the effective stress of coal fractures while the adsorption strain remains the same. Therefore, coal fractures are narrowed under the increasing effective stress, and the coal permeability ratio decreases by around 10%, from 1 to 0.9, as the red line shown in Figure 6b.

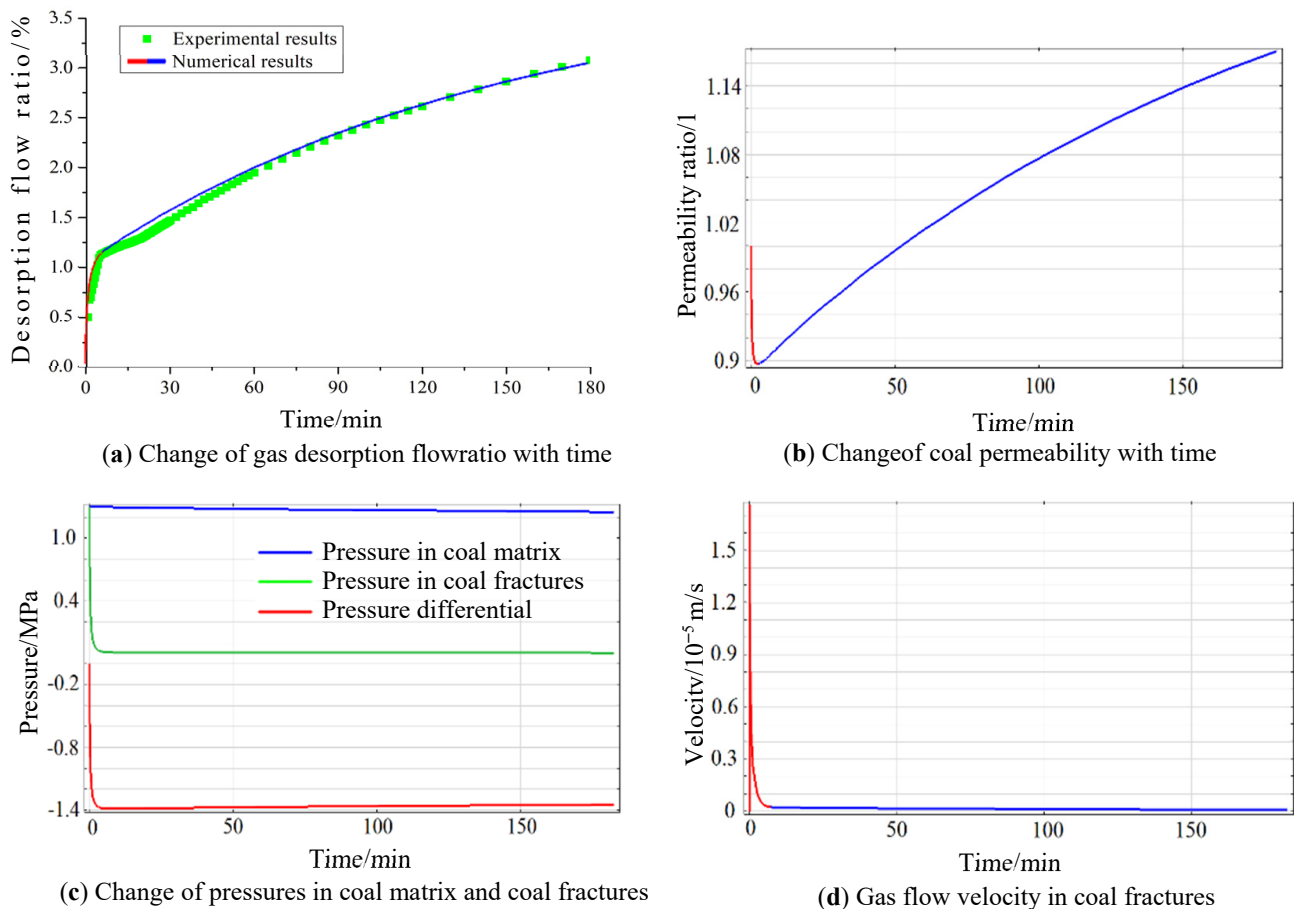


**Figure 6.** Numerical simulation results for Guhanshan coal.

**Table 2.** Basic numerical simulation parameters for Guhanshan coal.

Parameters	Values	Physical Meanings	Units
K	2410	Bulk modulus	MPa
$\varepsilon$	0.327	Poisson's ratio	-
$E_{m0}$	3850	Young's modulus of coal matrix	MPa
$E$	2498	Young's modulus of coal	MPa
$P_L$	1.54	Langmuir pressure constant	MPa
$\varepsilon_L$	0.06328	Langmuir volumetric strain constant	-
$k_{f0}$	0.096	Initial permeability of coal fractures	mD
$k_{m0}$	0.00096	Initial permeability of coal matrix	mD
$\varnothing_{f0}$	0.005	Initial porosity of coal fractures	-
$\varnothing_{m0}$	0.05	Initial porosity of coal matrix	-
$P_{ini}$	0.5, 1.0, 1.5	Initial equilibrium pressure in coal sample	MPa

At the second stage, as the red line shown in Figure 6c, the big pressure differential between coal fractures and coal matrix reaches 1.4 MPa due to the fast gas outflow in coal fractures and slow gas movement in coal matrix. This pressure differential causes methane to gradually desorb from coal matrix and flow to coal fractures. However, as the blue line shown in Figure 6d, the gas flow speed in coal fractures remains small,  $0.025 \times 10^{-5}$  m/s, which indicates that the methane flow from the coal matrix to coal fractures is very slow. As the gas pressure in the coal matrix decreases little, shown as the blue line in Figure 6c, the reason for the slow methane movement in the coal matrix can be deduced to be the low permeability of the coal matrix. Based on the theory on adsorption-induced deformation, the coal matrix shrinks during methane desorption, and this broadens the aperture of coal

fractures, which leads to an increase in the apparent coal permeability. Therefore, the coal permeability ratio gradually increases by around 28% in the later 174 min, from 0.9 to 1.18, shown as the blue line shown in Figure 6b. As analyzed above, the fast methane flow in coal fractures contributes to the quick increase in the desorption flow volume of methane at the first stage, while the slow methane migration in the coal matrix determines the gradual increase in the desorption flow volume of methane at the second stage.

According to the above analysis of the experimental results with the proposed tandem fracture-pore permeability model, gas flows in coal fractures and the coal matrix impose different but significant impacts on the evolution coal permeability. However, for much research, the effect of gas flow in coal fractures has not been well observed and analyzed with the effects of gas flow in the coal matrix. The experimental data from the literature are used to additionally validate and analyze the proposed tandem fracture-pore permeability model [40]. In this experiment, the coal samples were collected from the Anderson seam at the Powder River basin. Anderson coal is subbituminous and low-contaminant and is adopted for the measurement of coal permeability. As shown in Figure 7, the stress of 6.89 MPa was applied to the boundary of the coal sample, and methane was used for gas injection. The injection pressure increased from around 0.689 MPa to 5.512 MPa under the constant temperature of 300 K. For Anderson coal, the parameters that were used in the simulations are listed in Table 3. Since all the experimental data were collected at the final equilibrium stages in this experiment, the change in coal permeability reflects the effect of gas flow in the coal matrix on coal permeability without the influence of gas flow in the coal fractures.

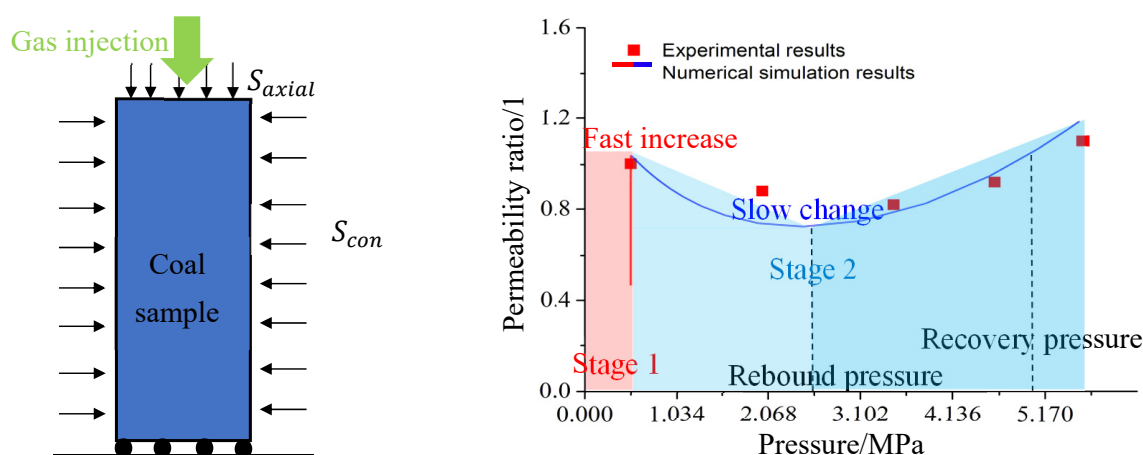


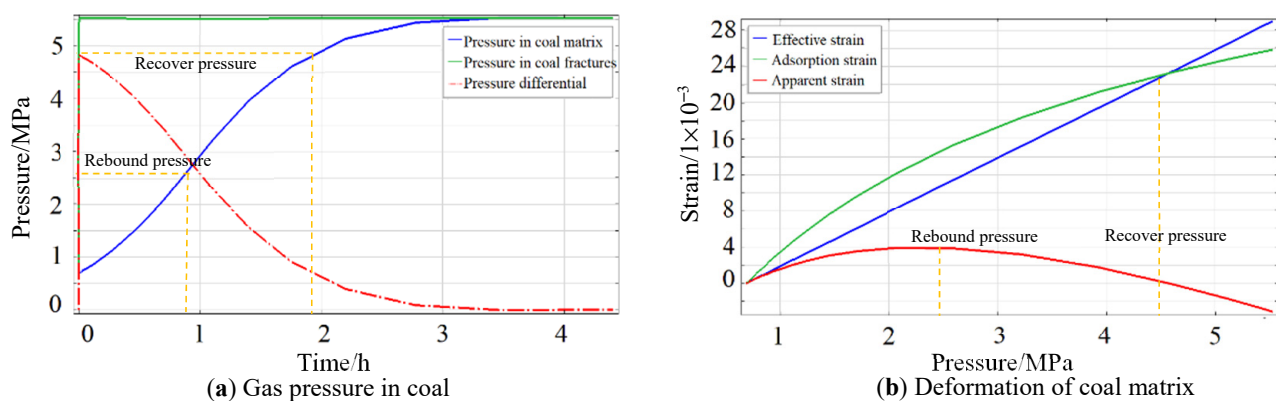
Figure 7. Experimental set-up and results for Anderson coal.

Table 3. Key parameters for Anderson coal in the numerical simulations [40].

Parameter	Value	Physical Meanings	Units
$E_{m0}$	4800	Young's modulus of coal matrix	MPa
$E$	2758	Young's modulus of coal	MPa
$P_L$	4.823	Langmuir pressure constant	MPa
$\varepsilon_L$	0.007	Langmuir volumetric strain constant	-
$k_{f0}$	0.0385	Initial permeability of coal fractures	mD
$k_{m0}$	0.0000385	Initial permeability of coal matrix	mD
$\varnothing_{f0}$	0.0045	Initial porosity of coal fractures	-
$\varnothing_{m0}$	0.045	Initial porosity of coal matrix	-

The experimental results and numerical simulation results for Anderson coal are shown in Figure 7. Based on the experimental results, it is clear that coal permeability experiences an increase after a decrease when methane is injected into coal. As the blue line shows in Figure 7, the coal permeability ratio first decreases from 1 at 0.551 MPa to

0.7 at 2.618 MPa and then increases to 1.15 at 5.512 MPa. Based on the tandem fracture-pore permeability model, the gradual change is mainly determined by the deformation of coal matrix. The changes in gas pressure and in coal matrix deformation are shown in Figure 8. During this gas injection process, the gas flow in the coal fractures reaches equilibrium quickly and the gas pressure holds at 5.512 MPa, while the gas pressure in the coal matrix begins to increase from 0.69 MPa. The obvious pressure differential of 4.8 MPa forms. Gas flow begins to intrude into the coal matrix. From Figure 8b, at the initial stage, the coal matrix swells to narrow coal fractures and lower coal permeability because the adsorption-induced strain of the coal matrix, shown as the blue line, is smaller than the effective strain of coal matrix, shown as the green line. The adsorption-induced strain of the coal matrix narrows the coal fractures, while the effective strain of the coal matrix broadens coal fractures and improve coal permeability. When gas pressure in the coal matrix reaches the rebound pressure of 2.618 MPa, the coal swelling reaches its maximum and the coal permeability decreases by 30% [22]. After this point, the adsorption-induced strain of coal matrix narrows begins to chase the effective strain of coal matrix with a bigger increase rate, and coal permeability begins to increase. When gas pressure in coal matrix reaches 4.565 MPa, the adsorption-induced strain of coal matrix equals the effective strain of coal matrix. As gas pressure in coal matrix reaches the recovery pressure of 4.545 MPa, coal permeability ratio recovers to 1. From this point, coal permeability ratio begins to be larger than 1 because the adsorption-induced strain of coal matrix is smaller than the effective strain of coal matrix.



**Figure 8.** Change of gas pressure and coal matrix deformation.

However, this experiment did not observe the change in coal permeability at the initial stage of gas injection. If the effective strain of coal fractures is considered, the complete change process of coal permeability includes the red line part shown in Figure 7. To conveniently compare the experimental results and numerical simulation results, the inflection point of the evolution curve of coal permeability ratio was moved to 1. Before the slowly increasing stage, the permeability of the Anderson coal quickly increased by around 55%, which means a fast jump. This fast jump of coal permeability is mainly caused by the injection-caused increase in the aperture of coal fractures. When gas is injected into coal, gas quickly flows in coal fractures and the gas pressure in coal fractures reaches its equilibrium in a short time. As the gas pressure in coal fractures increases, the effective strain of coal fractures decreases while gas adsorption in coal matrix has yet begun. As a result, the aperture of coal fractures is broadened and coal permeability increases in a short time. From Figure 9, the coal fracture aperture ratio increases by 14%, from 1 to 1.14, in the initial several minutes of gas injection. After that, coal fracture aperture is mainly influenced by the apparent coal matrix deformation.

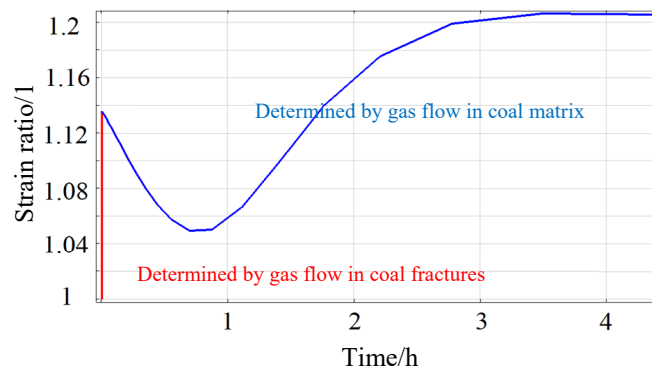


Figure 9. Deformation of coal fractures for Anderson coal.

5.2. Model Sensitivity Analysis

Based on the above analysis, the fast change as well as gradual change in coal permeability could be investigated using the proposed tandem fracture-pore permeability model for coal. In this model, the modulus of coal fractures was determined by the moduli of coal and coal matrix. To analyze the effect of gas flows on the change of coal permeability with different moduli of coal fractures and matrix, four coal samples of different physical properties were used for the numerical simulation. The initial conditions and boundary conditions were the same as the numerical simulation for Anderson coal, and the adsorption capacity remained the same as for the Anderson coal. The moduli for the coal and the coal matrix are listed in Table 4, and the simulation results are shown in Figure 10.

Table 4. Coal moduli for the numerical research on model sensitivity.

Young’s Modulus	Coal 1#	Coal 2#	Coal 3#	Coal 4#
$E$ /MPa	3000	2760	1800	2000
$E_{m0}$ /MPa	5200	4800	2850	4000
$E_{f0}$ /MPa	52	47	36	29

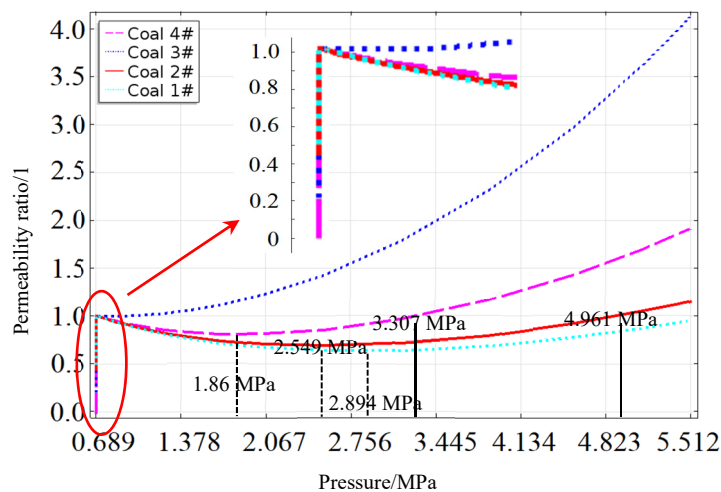


Figure 10. Permeability changes under different coal modulus.

As shown in Figure 10, coals of different physical properties show different changes in permeability. For coal 1# to 4#, Young’s modulus for coal fractures is 32 MPa, 29 MPa, 22 MPa and 18 MPa, respectively. At the initial stage, for coal 1# to 4#, the quick increase in gas pressure in coal fractures leads to increases in coal permeability by 51%, 57%, 80% and 100%, respectively. Although there are different moduli for these four coal samples, the fast change in coal permeability shows a negative relationship with Young’s modulus

of coal fractures. Then, coal permeability experiences a slow change with an apparently different slope. This inflection point is taken as a reference point for the permeability ratio of 1. At the second stage, coal permeability starts to decrease due to the dominant adsorption swelling except coal 3#. For coal 1#, 2# and 4#, the rebound pressure is 2.894 MPa, 2.549 MPa and 1.86 MPa, respectively [22]. Then, coal permeability increases because of the increasing compaction of coal matrix. The coal permeability for coal 1# recovers to 95% of the reference point at 5.512 MPa. For coal 2# and 4#, coal permeability increases by 15% and 91%, respectively, and their recovery pressure is 4.961 MPa and 3.307 MPa, respectively [22]. For coal 3#, Young's modulus of coal matrix is small, and this leads to the dominant shrinkage of coal matrix. Therefore, coal permeability keeps increasing all the time, and it increases by 313% at 5.512 MPa.

Based on the numerical simulation results, the fast jump in coal permeability is related to the effective strain of the 'soft' coal fracture part, which is influenced by moduli of coal and coal matrix. The gradual change in coal permeability is related to the strain of the 'hard' coal matrix, which is determined by the effective strain and adsorption-deformation capacity and modulus of coal matrix. Therefore, the permeability of coal of different mechanical properties and adsorption capacities constitutes a coal permeability map including various evolution routines [33]. This explains the different change trend of coal permeability even under the same experimental conditions.

### 5.3. Analysis on Methane Drainage Process

The fast decrease in gas drainage volume is an important engineering problem for CBM development and prevention of methane accidents in coal mines. Taking Anderson coal as an example, the initial gas pressure and drainage pressure were set to be 3 MPa and 0.1 MPa, respectively, to analyze methane flow during the methane drainage process with the proposed tandem fracture-pore permeability model [40–42].

The changes in gas pressure in Anderson coal under the drainage condition are shown in Figure 11. The numerical simulation results indicate that the gas in coal fractures quickly flows out during methane drainage. Within the first 2 min, the gas pressure in coal fractures, as the green line shown, decreased from the initial 3 MPa to around 0.74 MPa with a big slope, which means a fast gas outflow; gas pressure of 0.74 MPa is one indicator of the disaster risk of coal and gas outburst in coal mines in China. Thereafter, the gas pressure in coal fractures slowly decreased to the drainage pressure of 0.1 MPa in one hour with a moderate slope. Corresponding to the different stages of the gas pressure in coal fractures, the gas pressure in the coal matrix, shown as the blue line, shows little change in the first 2 min with a small slope. At this stage, a big gas pressure difference between coal fractures and coal matrix formed, shown as the red line. The gas pressure difference reached the maximum of 2.4 MPa at this moment. Then, the gas pressure in the coal matrix began to decrease from around 3 MPa to 0.74 MPa with a steep slope in the later 3 h. In this stage, the pressure differential between coal fractures and the coal matrix promoted gas mass exchange to speed the gas flow in coal matrix. However, this gas mass exchange was not big or fast enough, which caused it to take a long time for the gas pressure in the coal matrix to decrease to 0.74 MPa. After this stage, the gas pressure in the coal matrix experienced a moderate decline and decreased to the drainage pressure of 0.1 MPa in another 77 h. In this stage, the small and slow gas mass exchange between coal fractures and coal matrix further weakened when the gas pressure difference decreased to zero.

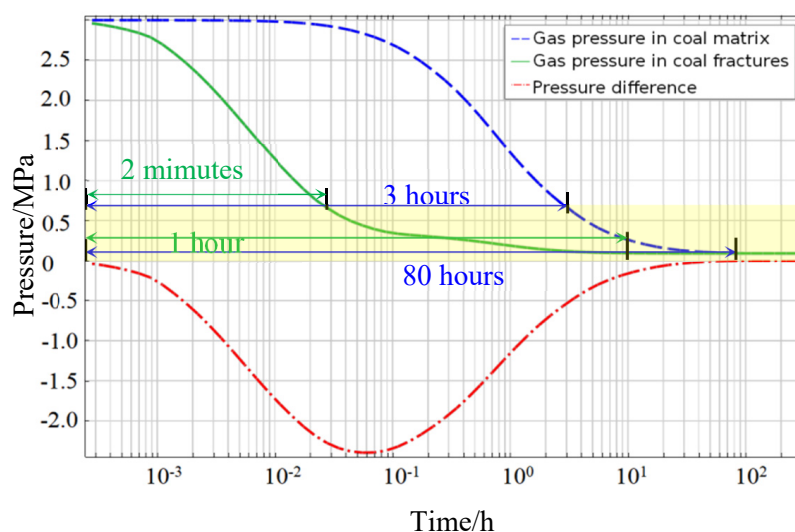


**Figure 11.** Gas pressure changes for Anderson coal under drainage condition.

The evolution of coal permeability for Anderson coal under the methane drainage condition is shown in Figure 12. At the beginning, coal permeability shows a reduction of 10% in a short time. This decrease in coal permeability is caused by the fast decreasing gas pressure in coal fractures. In the first 2 min, the gas pressure in coal fractures decrease to 0.74 MPa, which leads to the quick compression of coal fractures and the decrease in coal permeability. After that, coal permeability experiences another sharp decrease of 10% when the gas pressure in coal matrix decreases to around 2.7 MPa. In this stage, the gas pressure difference between coal fractures and coal matrix gradually reaches maximum. However, the low permeability of coal matrix leads to the slow and insufficient mass exchange between coal matrix and coal fractures. The effective strain of coal fractures changes slightly due to the small change in gas pressure in coal fractures. In the contrary, the change in the adsorption-induced strain of coal matrix increases to lower coal porosity and coal permeability. Thereafter, coal permeability ratio slowly decreases to around 0.55 during a long time period. In this period, the change in the effective strain of coal matrix is bigger than the change in the adsorption-induced strain of coal matrix, which means the effective strain of coal matrix dominants in coal deformation. This explains the long-time and slow decrease in coal permeability. The fast and dramatic decrease in coal permeability caused by coal fractures causes the quick reduction in gas production, and the further slow decrease in coal permeability results in the low efficiency of gas drainage. This research results can be supported by the change of gas production rate measured from the well in developed coalbed methane reservoirs [43]. For the exploration of gas hydrate, this change process of reservoir permeability can be used to analyze the gas flow process of gas hydrate in the hydrate-bearing sediments for explaining the similar gas production rate. Although the deformation characteristics of fractures and tight medium are similar, there is difference between the physical properties of fluid gas and gas hydrate. The effects of hydrate phase and phase transition on coal deformation should be considered to better understand its flow process [44].

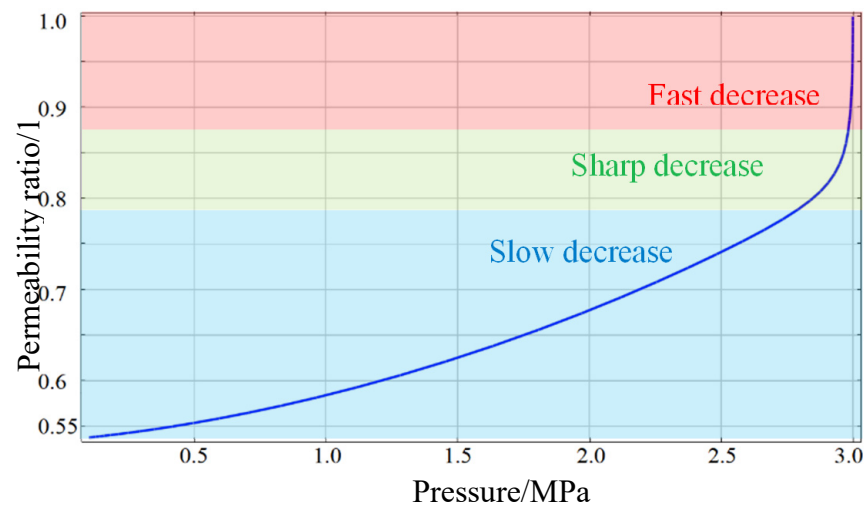


Figure 12. Permeability change for Anderson coal under drainage condition.

## 6. Conclusions

Based on the characteristics of gas flows in porous coal, a tandem fracture-pore permeability model is proposed and validated with experimental results. Different from the previous coal permeability models, the deformation of coal fractures is determined by its loading environment and adsorption environment rather than the derivation of the deformation of the coal and the coal matrix. After the analysis of the evolution of coal permeability under injection and drainage conditions with this proposed coal permeability, the conclusions are summarized as below,

(1) Coal fractures may have strength to resist coal deformation. Based on the validated numerical simulation results, the smaller strength of ‘soft’ coal fractures can quickly and significantly resist swelling and shrinkage of coal fractures during gas injection and gas drainage process. This causes the great but short time gas flow and greater coal permeability. Based on the series springs model, Young’s modulus of coal fractures can be determined theoretically.

(2) The complete evolution of coal permeability includes both the fast change caused by gas flow in coal fractures and the gradual change caused by gas migration in coal matrix. The fast gas flow in coal fractures causes quick change in coal permeability due to the effective strain of coal fractures. The slow gas migration in coal matrix determines the gradual change in coal permeability at the later stage owing to the effective strain and adsorption-induced strain of coal matrix.

(3) The low efficiency of gas mass exchange between coal fractures and coal matrix causes unusual change in gas flow in coal. After fast gas outflow from coal fractures, there is insufficient gas supplement from the coal matrix due to ultra-low coal matrix permeability even under an obvious pressure differential. This explains the quick reduction in gas production after a good but short performance for CBM development.

## 7. Further Research

Hydraulic measures are popular to improve coal permeability for a better CBM production. Coal matrix and coal fractures may show different deformation characteristics when water is injected into coal. As water can be considered to be incompressible, this may cause coal permeability to show different change routine, which is significant for CBM improvement by hydraulic measures. Therefore, the deformation characteristics of coal under the condition of high-pressure water injection needs to be studied in the future.



**Author Contributions:** Conceptualization, L.L.; Formal analysis, L.L.; Writing—original draft, L.L.; Methodology, L.L.; Funding acquisition, L.L., Z.L. and X.C.; Writing—editing, S.Z. and S.F.; Validation, S.Z. and S.F.; Methodology—review, Z.L. and L.W.; Supervision, Z.L. and X.C.; Resources, X.C. All authors have read and agreed to the published version of the manuscript.

**Funding:** This study was supported by the National Natural Science Foundation of China (No. 52074105; No. 51874122), the Program for Innovative Research Team of Henan Polytechnic University (No. T2019-4), the Fundamental Research Funds for the Universities of Henan Province (No. NSFRF180305), the Open Subject of State Key Laboratory of Coal Mine Disaster Dynamics Control (No. 2011DA105287-KF201313), the Program for Changjiang Scholars and Innovative Research Team (No. PCSIRT1235), the Doctoral Foundation of Henan Polytechnic University (B2021-7), the State Key Laboratory Cultivation Base for Gas Geology and Gas Control (Henan Polytechnic University) (No. WS2021A06), the Key Scientific Research Projects of Colleges and Universities in Henan Province (No. 22B620002), the Key Science and Technology Project of Henan Province (No. 222102320017), and the China Scholarship Council (No. 201706420010; No. 201808410203).

**Data Availability Statement:** The data presented in this study are available on request from the corresponding author.

**Conflicts of Interest:** The authors declare that they have no known competing financial interest or personal relationships that could have appeared to influence the work reported in this paper.

## References

1. Xu, C.; Yang, G.; Wang, K.; Fu, Q. Uneven stress and permeability variation of mining disturbed coal seam for targeted CBM drainage: A case study in Baode coal mine. eastern Ordos Basin, China. *Fuel* **2021**, *289*, 119911. [[CrossRef](#)]
2. Xu, C.; Cheng, Y.P.; Ren, T.X.; Wang, L.; Kong, S.L.; Lu, S.Q. Gas ejection accident analysis in bed splitting under igneous sills and the associated control technologies: A case study in the Yangliu Mine, Huaibei Coalfield, China. *Nat. Hazards* **2014**, *71*, 109–134. [[CrossRef](#)]
3. Zhang, C.L.; Xu, J.; Peng, S.J.; Li, Q.X.; Yan, F.Z.; Chen, Y.X. Dynamic behavior of gas pressure and optimization of borehole length in stress relaxation zone during coalbed methane production. *Fuel* **2018**, *233*, 816–824. [[CrossRef](#)]
4. Durucan, S.; Edwards, J.S. The effects of stress and fracturing on permeability of coal. *Min. Sci. Technol.* **1986**, *3*, 205–216. [[CrossRef](#)]
5. Palmer, I.; Mansoori, J. How permeability depends on stress and pore pressure in coalbeds: A new model. In Proceedings of the SPE Annual Technical Conference and Exhibition, Denver, CO, USA, 6 October 1996.
6. Seidle, J.P.; Jeanson, M.W.; Erickson, D.J. Application of matchstick geometry to stress dependent permeability in coals. In Proceedings of the SPE Rocky Mountain Regional Meeting, Casper, WY, USA, 18 May 1992.
7. Liu, J.S.; Chen, Z.W.; Elsworth, D.; Miao, X.X.; Mao, X.B. Evaluation of stress-controlled coal swelling processes. *Int. J. Coal Geol.* **2010**, *83*, 446–455. [[CrossRef](#)]
8. Salmachi, A.; Rajabi, M.; Wainman, C.; Mackie, S.; McCabe, P.; Camac, B.; Clarkson, C. History, Geology, In Situ Stress Pattern, Gas Content and Permeability of Coal Seam Gas Basins in Australia: A Review. *Energies* **2021**, *14*, 2651. [[CrossRef](#)]
9. Skoczylas, N.; Dutka, B.; Sobczyk, J. Mechanical and gaseous properties of coal briquettes in terms of outburst risk. *Fuel* **2014**, *134*, 45–52. [[CrossRef](#)]
10. Zhang, C.L.; Wang, E.Y.; Xu, J.; Peng, S.J. A new method for coal and gas outburst prediction and prevention based on the fragmentation of ejected coal. *Fuel* **2021**, *287*, 119493. [[CrossRef](#)]
11. Pan, Z.J.; Connell, L.D. Modelling permeability for coal reservoirs: A review of analytical models and testing data. *Int. J. Coal Geol.* **2012**, *92*, 1–44. [[CrossRef](#)]
12. Warren, J.E.; Root, P.J. The behavior of naturally fractured reservoirs. *Sot. Pet. Eng. J.* **1963**, *3*, 245–255. [[CrossRef](#)]
13. Pirson, S.J. Performance of fractured oil reservoirs. *AAPG Bull.* **1953**, *37*, 232–244.
14. Zhao, S.; Chen, X.J.; Li, X.J.; Qi, L.L.; Zhang, G.X. Experimental analysis of the effect of temperature on coal pore structure transformation. *Fuel* **2021**, *305*, 121613. [[CrossRef](#)]
15. Ni, Z.; Lin, B.Q.; Zhang, X.L.; Cao, X.; Zhong, L.B.; Gao, Y.B. Experimental study on the effect of high-voltage electrical pulses on the nanoscale pore structure of coal. *Fuel* **2021**, *306*, 121621. [[CrossRef](#)]
16. Zheng, S.J.; Yao, Y.B.; Elsworth, D.; Wang, B.; Liu, Y. A novel pore size classification method of coals: Investigation based on NMR relaxation. *J. Nat. Gas Sci. Eng.* **2020**, *81*, 103466. [[CrossRef](#)]
17. Zeng, J.; Li, W.; Liu, J.S.; Leong, Y.K.; Elsworth, D.; Tian, J.W.; Guo, J.C.; Zeng, F.H. Analytical solutions for multi-stage fractured shale gas reservoirs with damaged fractures and stimulated reservoir volumes. *J. Petrol. Sci. Eng.* **2020**, *187*, 106686. [[CrossRef](#)]
18. Li, W.; Liu, J.S.; Zeng, J.; Leong, Y.K.; Elsworth, D.; Tian, J.W.; Li, L. A fully coupled multidomain and multiphysics model for evaluation of shale gas extraction. *Fuel* **2020**, *278*, 118214. [[CrossRef](#)]
19. Li, Z.Q.; Peng, J.S.; Li, L.; Qi, L.L.; Li, W. Novel Dynamic Multiscale Model of Apparent Diffusion Permeability of Methane through Low-Permeability Coal Seams. *Energy Fuel* **2021**, *35*, 7844–7857. [[CrossRef](#)]

20. Song, W.H.; Yao, B.W.; Yao, J.; Li, Y.; Sun, H.; Yang, Y.F.; Zhang, L. Methane surface diffusion capacity in carbon-based capillary with application to organic-rich shale gas reservoir. *Chem. Eng. J.* **2018**, *352*, 644–654. [\[CrossRef\]](#)
21. Barenblatt, G.I.; Zheltov, L.P.; Kochina, I.N. Basic concepts on the theory of seepage of homogeneous liquids in fissured rocks. *J. Appl. Math. Mec.* **1960**, *24*, 1286–1303. [\[CrossRef\]](#)
22. Cui, X.J.; Bustin, R.M. Volumetric strain associated with methane desorption and its impact on coalbed gas production from deep coal seams. *AAPG Bull.* **2005**, *89*, 1181–1202. [\[CrossRef\]](#)
23. Mojgan, H.M.; Matthew, T.; Majid, S.; Philip, J.V. Carbon dioxide flow and interactions in a high rank coal: Permeability evolution and reversibility of reactive processes. *Int. J. Greenh. Gas Con.* **2018**, *70*, 57–67.
24. Liu, C.J.; Wang, G.; Sang, S.; Rudolph, V. Changes in pore structure of anthracite coal associated with CO<sub>2</sub> sequestration process. *Fuel* **2010**, *89*, 2665–2672. [\[CrossRef\]](#)
25. Fan, C.J.; Elsworth, D.; Li, S.; Zhou, L.J.; Yang, Z.H.; Song, Y. Thermo-hydro-mechanical-chemical couplings controlling CH<sub>4</sub> production and CO<sub>2</sub> sequestration in enhanced coalbed methane recovery. *Energy* **2019**, *173*, 1054–1077. [\[CrossRef\]](#)
26. Gensterblum, Y.; Ghanizadeh, A.; Krooss, B.M. Gas permeability measurements on Australian subbituminous coals: Fluid dynamic and poroelastic aspects. *J. Nat. Gas Sci. Eng.* **2014**, *19*, 202–214. [\[CrossRef\]](#)
27. Li, S.; Dong, M.; Li, Z. Measurement and revised interpretation of gas flow behaviour in tight reservoir cores. *J. Petrol. Sci. Eng.* **2009**, *65*, 81–88. [\[CrossRef\]](#)
28. Kumar, H.; Elsworth, D.; Mathews, J.P.; Marone, C. Permeability evolution insorbing media: Analogies between organic-rich shale and coal. *Geofluids* **2016**, *16*, 43–55. [\[CrossRef\]](#)
29. Kwon, O.; Kronenberg, A.K.; Gangi, A.F.; Johnson, B. Permeability of Wilcox shale and its effective pressure law. *J. Geophys. Res.* **2001**, *106*, 339–353. [\[CrossRef\]](#)
30. Yun, Z.; Jianfang, S.; Zhongchun, L. Study of numerical simulation method modelling gas injection into fractured reservoirs. *Min. Miner. Depos.* **2019**, *13*, 41–45. [\[CrossRef\]](#)
31. Zhang, H.B.; Liu, J.S.; Elsworth, D. How sorption-induced matrix deformation affects gas flow in coal seams: A new FE model. *Int. J. Rock Mech. Min.* **2008**, *45*, 1226–1236. [\[CrossRef\]](#)
32. Harpalani, S. *Gas Flow through Stressed Coal*; California University: Berkeley, CA, USA, 1985.
33. Zhang, S.W.; Liu, J.S.; Wei, M.Y.; Elsworth, D. Coal permeability maps under the influence of multiple coupled processes. *Int. J. Coal Geol.* **2018**, *187*, 71–82. [\[CrossRef\]](#)
34. Golf-Racht, V.T.D. *Fundamentals of Fractured Reservoir Engineering*; Elsevier Scientific Publishing Company: Amsterdam, The Netherlands, 1982.
35. Liu, H.H.; Rutqvist, J.; Berryman, J.G. On the relationship between stress and elastic strain for porous and fractured rock. *Int. J. Rock Mech. Min.* **2009**, *46*, 289–296. [\[CrossRef\]](#)
36. Berryman, J.G. Estimates and rigorous bounds on pore-fluid enhanced shear modulus in poroelastic media with hard and soft anisotropy. *Int. J. Damage Mech.* **2006**, *15*, 133–167. [\[CrossRef\]](#)
37. Mavko, G.; Jizba, D. Estimating grain-scale fluid effects on velocity dispersion in rocks. *Geophysics* **1991**, *56*, 1940–1949. [\[CrossRef\]](#)
38. Cheng, A.H.D. *Poroelasticity*; Springer: Cham, Switzerland, 2016.
39. Wei, M.Y.; Liu, J.S.; Shi, R.; Elsworth, D.; Liu, Z.H. Long-Term evolution of coal permeability under effective stresses gap between matrix and fracture during CO<sub>2</sub> injection. *Transp. Porous Media* **2019**, *130*, 969–983. [\[CrossRef\]](#)
40. Robertson, E.P. Measurement and modeling of sorption-induced strain and permeability changes in coal. *Colo. Sch. Mines. Arthur Lakes Libr.* **2005**, 31–112.
41. Lou, Z.; Wang, K.; Zang, J.; Zhao, W.; Qin, B.B.; Kan, T. Effects of permeability anisotropy on coal mine methane drainage performance. *J. Nat. Gas Sci. Eng.* **2021**, *86*, 103733. [\[CrossRef\]](#)
42. Wiesław, S.; Małgorzata, S.V.; Andrzej, G.; Krzysztof, P. Numerical studies of improved methane drainage technologies by stimulating coal seams in multi-seam mining layouts. *Int. J. Rock Mech. Min.* **2018**, *108*, 157–168.
43. Salmachi, A.; Bonyadi, M.R.; Sayyafzadeh, M.; Haghghi, M. Identification of potential locations for well placement in developed coalbed methane reservoirs. *Int. J. Coal Geol.* **2014**, *131*, 250–262. [\[CrossRef\]](#)
44. Zhang, J.; Liu, X.; Chen, D.; Yin, Z. An investigation on the permeability of hydrate-bearing sediments based on pore-scale CFD simulation. *Int. J. Heat Mass Transf.* **2022**, *192*, 122901. [\[CrossRef\]](#)